A *WISE* view of *IRAS* debris disks: revising the dust properties

Qiong Liu

Department of Physics, Guizhou University, Guiyang 550025, China; *qliu1@gzu.edu.cn*

Abstract Debris disks around stars are considered as components of planetary systems. Constraining the dust properties of these disks can give crucial information to formation and evolution of planetary systems. As an all-sky survey, *InfRared Astronomical Satellite* (*IRAS*) gave great contribution to the debris disk searching which discovered the first debris disk host star (Vega). The *IRAS*-detected debris disk sample published by Rhee (Rhee et al. 2007) contains 146 stars with detailed information of dust properties. While the dust properties of 45 of them still cannot be determined due to the limitations with the *IRAS* database (have *IRAS* detection at 60 μm only). Therefore, using more sensitivity data of *Wide-field Infrared Survey Explorer* (*WISE*), we can better characterize the sample stars: for the stars with *IRAS* detection at 60 μm only, we refit the excessive flux densities and obtain the dust temperatures and fractional luminosities; while for the remaining stars with multi-bands *IRAS* detections, the dust properties are revised which show that the dust temperatures were overestimated in the high temperature band before. Moreover, we identify 17 stars with excesses at the *WISE* 22 μm which have smaller distribution of distance from Earth and higher fractional luminosities than the other stars without mid-infrared excess emission. Among them, 15 stars can be found in previous works.

Key words: (stars:) circumstellar matter — protoplanetary disks — infrared: stars

1 INTRODUCTION

Debris disks are almost dust-dominated and surround their stars with a wide age range (Hughes et al. 2018). The dust is usually not primordial because its lifetime was much shorter than the stellar age (Wyatt 2018). Debris disks are considered as planetary system components or protoplanetary disk descendants, which provides a wealth of valuable information on evolution of circumstellar disks and planet formation outcome (Wyatt et al. 2017).

Since *IRAS* first discovered Vega with debris disk in 1984 (Auman et al. 1984), attempts of searching debris disk candidates are never stopped. The most effective way of searching debris disks is to detect the infrared (IR) excess with IR radiation exceeds the stellar photospheric radiation The dust surrounds the sample stars and reaches a thermal equilibrium under stellar radiation, then it will re-emit the light absorbed from the host star at IR to sub-millimeter (Krivov 2010).

Up to now, many hundreds of debris disks have been discovered (Wyatt 2018). They are based on five satellites as follows: *IRAS* (Rhee et al. 2007; Mannings & Barlow 1998), *Infrared Space Observatory* (*ISO*) (Oudmaijer et al. 1992; Kessler et al. 1996; Abraham et al. 1999; Fajardo et al. 1999; Habing et al. 1999; Spangler et al. 2001; Decin et al. 2003), *Spitzer* (Chen et al. 2005; Rieke et al. 2005; Kim et al. 2005; Su et al. 2006; Beichman et al. 2006; Moór et al. 2006; Bryden et al. 2006; Siegler et al. 2007; Rebull et al. 2008; Moór et al. 2011; Wu et al. 2012; Chen et al. 2014; Mittal et al. 2015; Ballering et al. 2018), *Herschel* (Matthews et al. 2010; Eiroa et al. 2013; Dodson-Robinson et al. 2016; Vican et al. 2016; Sibthorpe et al. 2018), and *AKARI* (Fujiwara et al. 2013; Liu et al. 2014; Ishihara et al. 2017). Among these surveys, *IRAS* and *AKARI* are all-sky surveys and the other three (*Spitzer*, *ISO* and *Herschel*) are not. Though with much smaller area covering, the latter three missions have much better sensitivities and spatial resolutions so that they can detect more faint disks.

However, *IRAS* and *AKARI* still have their own advantages because of their all-sky area. Although both *IRAS* and *AKARI* are all-sky surveys, the debris disk candidates detected by them are not exactly the same. The debris disk sample of Rhee (Rhee et al. 2007) detected by *IRAS* contains 146 stars with debris disk candidates via cross-correlating the *IRAS* Point Source Catalog (PSC) and Faint Source Catalog (FSC) with the *Hipparcos*

main sequence star catalog. The debris disk sample of Liu (Liu et al. 2014) detected by *AKARI* contains 72 stars debris disk candidates via cross-correlating the AKARI/Far-Infrared Surveyor (Kawada et al. 2007) All-Sky Survey Bright Source Catalogue (AKARIBSC, Yamamura et al. 2010) with the *Hipparcos* main sequence star catalog. Among these two samples, 27 stars are in common although they have the similar sensitivity (*IRAS* at 60 μm band and *AKARI/FIS* at 90 μm). Most of the sources in Rhee's sample cannot be detected by *AKARI/FIS* because of its shallow limit. So Rhee's sample still has its own value.

The sample of Rhee gives dust properties of debris disks including dust temperature, fractional luminosity and dust mass. It presents a good sample for other works, such as follow-up observations of debris disks (*Herschel*: Marshall et al. 2013; Vican et al. 2016, *Spitzer*: Chen et al. 2014; Mittal et al. 2015, *ALMA*: Booth et al. 2019 and Submillimeter: Bulger et al. 2013; Holland et al. 2017); debris disks around A-type stars (Greaves et al. 2016; Welsh & Montgomery 2018; Moór et al. 2017); Individual disk research (Fujiwara et al. 2009; Borgniet et al. 2014; Hung et al. 2015; Su et al. 2015; Konopacky et al. 2016; Geiler et al. 2019). Moreover, this sample focuses on debris disk evolution which gives great guidance to evolution works of other people (Wyatt et al. 2007; Moór et al. 2011; Vican & Schneider 2014). This sample is also helpful to other statistical works: metallicity (Maldonado et al. 2012), binaries (Rodriguez & Zuckerman 2012), Kuiper Belts (Nilsson et al. 2010) and so on.

However, the dust properties of 45 of them still cannot be determined due to the limitations with the *IRAS* database: these stars have only *IRAS* 60 μm detection. This limitation can be broken through with more sensitivity observation data of *Wide-field Infrared Survey Explorer* (*WISE*). Many studies have used *WISE* to search for IR excess stars (Cotten & Song 2016; Wu et al. 2013, 2016). *WISE* makes an all-sky survey at four IR bands with $W1$ at 3.4 μm, $W2$ at 4.6 μm, $W3$ at 12 μm and $W4$ at 22 μm. The angular resolutions of corresponding bands are $6''.1$, $6''.4$, $6''.5$ & $12''$ and the 5σ point source sensitivities of corresponding bands are better than 0.08, 0.11, 1 and 6 mJy. For high signal-to-noise ratio sources, the astrometry precision is better than $0''.15$ (Wright et al. 2010). The flux densities of $W1$ and $W2$ can be used to test the fitting quality of model spectra. The flux densities of $W3$ and $W4$ can be used to fit the dust components and revise the properties.

This paper has refitted the Spectral Energy Distributions (SEDs) of Rhee's sample stars and refitted the excessive flux densities with *WISE* all-sky source catalog and *IRAS* catalog to revise the dust properties

and get Mid-IR excess information. The sample and photosphere emission are described in Section 2 and results and analysis including the properties of debris disks and hosting stars as well as *WISE* 22 μm excess are presented in Section 3. I will discuss the revised dust properties and Mid-IR excess sample in Section 4 and draw the summary in Section 5.

2 THE SAMPLE AND PHOTOSPHERE EMISSION

2.1 The Sample

The sample used in this work is debris disks of 146 stars within 120 pc of Earth detected by *IRAS* (Rhee et al. 2007), which cross-correlate the *IRAS* Point Source Catalog (PSC) and Faint Source Catalog (FSC) with the *Hipparcos* main sequence star catalog. *IRAS* makes an all-sky survey at four bands centered at 12, 25, 60, and 100 μm (Neugebauer et al. 1984). The *Hipparcos* main sequence star catalog has more than 110 000 stars with the information of photometry and astrometry for the nearby stars (Bessell 2000).

All stars have debris disks around, which are identified by excesses at *IRAS* 60 μm as described in the paper of Rhee. We will check these results in the Section 3. Note that three stars were removed from the sample: two pre-main-sequence stars (HIP 53911, HIP 77542) and one star (HIP 19704) with a detection at 60 μm flux quality of 1 (which means the flux quality is not reliable). The sample has 143 stars left over.

2.2 The Photosphere Emission

It is essential to obtaining the 143 sample stars' photosphere flux densities in order to identify and measure the IR excess strength (Bryden et al. 2006). To construct the SEDs, we collected the optical data (B and V from the *Hipparcos* satellite measurements) to near-infrared (NIR) absolute photometric data (JHK_s from Two Micron All Sky Survey (*2MASS*) catalog) for all sample stars (Skrutskie et al. 2006) and converted these observed magnitudes into flux density (Janskys) by using the zero magnitudes in Cox & Pilachowski (2000). The photometry of the sample stars are listed in Table 1. Then we use Kurucz' models (ATLAS9, Castelli & Kurucz 2004) to fit the stellar SEDs as our previous work do (Liu et al. 2014). The best model was selected out with the minimum χ^2 which are presented in Table 1.

3 RESULTS AND ANALYSIS

With the best-fit Kurucz model, we can estimate the flux densities of stellar photosphere in the corresponding *WISE* and *IRAS* bands. We check the *IRAS* excesses of

Table 1 Photometry and Flux Density for the 140 Sample Stars

HIP	B	V	J	H	K	w1m	w2m	w3m	w4m	f12	f25	f60	f100	χ^2
	mag	mag	mag	mag	mag	mag	mag	mag	mag	Jy	Jy	Jy	Jy	
(1)	(2)	(3)	(4)	(5)	(6)	(7)	(8)	(9)	(10)	(11)	(12)	(13)	(14)	(15)
746	2.66	2.28	1.71	1.58	1.45	-0.876	-0.178	1.462	1.335	11.700	2.871	1.001	12.660	5.85e-01
1185	7.08	6.82	6.38	6.31	6.25	6.191	6.142	6.284	6.228	0.175	0.167	0.211	0.567	4.46e-03
4267	5.78	5.80	5.74	5.80	5.80	5.801	5.734	5.825	5.454	0.193	0.149	0.174	1.309	1.00e-03
5626	5.61	5.60	5.46	5.50	5.49	5.535	5.388	5.493	4.656	0.260	0.111	0.403	2.081	3.22e-02
6686	2.82	2.66	2.34	2.37	2.25	0.834	0.793	2.378	2.286	4.961	1.142	0.346	6.092	2.11e+00
6878	7.17	6.66	5.69	5.49	5.42	5.443	5.256	5.441	5.321	0.310	0.112	0.285	1.045	2.60e-01
7345	5.69	5.62	5.49	5.53	5.46	5.471	5.302	5.340	3.742	0.335	0.384	2.018	1.883	4.48e+00
7805	8.04	7.62	6.84	6.69	6.63	6.619	6.592	6.598	6.040	0.119	0.093	0.140	0.646	1.55e-01
7978	6.07	5.52	4.79	4.40	4.34	4.171	3.913	4.220	3.954	0.814	0.282	0.815	1.075	1.04e+01
8122	6.98	6.73	6.26	6.19	6.17	6.154	6.100	6.183	5.640	0.141	0.107	0.348	0.607	1.49e-02
8241	5.07	5.04	4.99	5.03	4.96	4.932	4.717	4.984	4.594	0.405	0.163	0.299	0.616	4.44e+00
9570	5.53	5.50	5.35	5.38	5.33	5.246	5.078	5.345	5.069	0.356	0.184	0.293	0.829	2.03e-01
10054	6.17	6.05	5.75	5.76	5.69	5.741	5.607	5.695	5.523	0.206	0.050	0.153	1.161	1.52e-01
10670	4.05	4.03	3.80	3.86	3.96	3.952	3.643	3.989	3.510	1.066	0.367	0.791	0.831	2.86e+00
11360	7.19	6.79	6.03	5.86	5.82	5.814	5.646	5.778	5.269	2.130	0.868	0.441	0.663	6.70e-01
11486	5.60	5.29	5.08	4.82	4.59	4.574	4.380	4.618	4.381	0.549	0.192	0.282	0.655	6.85e+00
11847	7.83	7.47	6.70	6.61	6.55	6.544	6.520	6.503	4.236	0.125	0.177	0.868	0.853	8.35e-01
12361	7.17	6.78	6.11	5.97	5.92	5.955	5.799	5.904	5.406	0.157	0.086	0.304	0.768	6.26e+00
12964	6.87	6.48	5.76	5.63	5.57	5.554	5.357	5.585	5.457	0.253	0.140	0.226	0.630	1.00e-01
13005	9.03	8.06	6.42	5.99	5.88	5.887	5.842	5.913	5.859	0.138	0.245	0.288	1.013	1.24e+00
13141	5.35	5.25	5.14	5.16	4.97	4.963	4.748	5.012	4.781	0.414	0.097	0.164	0.490	1.66e+00
14576	2.09	2.09	1.96	1.95	1.89	-0.011	0.244	1.903	1.782	7.348	1.866	0.455	1.685	5.20e-01
15197	5.03	4.80	4.42	4.25	4.22	4.149	3.869	4.135	4.102	0.848	0.235	0.214	1.566	4.04e+00
16449	6.50	6.38	6.16	6.12	6.10	6.097	6.045	6.115	5.372	0.173	0.101	0.595	0.636	1.04e-01
16537	4.60	3.72	2.23	1.88	1.78	2.970	2.285	1.770	1.288	9.672	2.667	1.631	2.008	4.95e+00
18437	6.91	6.89	6.85	6.87	6.86	6.851	6.868	6.705	5.118	0.101	0.080	0.183	0.446	1.98e+00
18859	5.90	5.38	4.71	4.34	4.18	4.146	3.926	4.289	3.882	0.982	0.247	0.287	2.242	7.76e-02
18975	5.82	5.45	4.81	4.58	4.51	4.529	4.269	4.530	4.442	0.639	0.262	0.209	1.923	6.27e-01
19704	7.31	6.99	6.34	6.29	6.18	6.093	5.945	6.160	6.060	0.131	0.050	0.239	0.938	1.78e+00
19893	4.57	4.26	3.68	3.47	3.51	3.487	3.188	3.497	3.399	1.661	0.441	0.321	1.000	1.07e-01
20635	4.35	4.21	4.09	4.06	4.08	3.929	3.563	null	3.830	1.115	0.310	0.353	4.666	5.30e-04
21604	5.83	5.85	5.66	5.59	5.56	5.758	5.515	5.603	5.391	0.235	0.173	0.637	7.072	1.97e-02
22226	8.24	7.85	7.10	6.95	6.89	6.872	6.867	6.867	6.000	0.092	0.066	0.274	0.478	1.23e-01
22439	6.73	6.27	5.38	5.20	5.08	5.102	4.927	5.146	4.997	0.387	0.091	0.191	1.011	1.14e-01
22845	4.72	4.64	4.85	4.52	4.42	4.414	4.166	4.432	4.058	0.696	0.270	0.411	5.217	5.62e+00
23451	8.33	8.13	7.69	7.62	7.59	7.595	7.629	6.924	3.952	0.114	0.211	1.122	1.592	1.17e-29
24528	6.90	6.76	6.50	6.43	6.43	6.408	6.371	6.357	5.589	0.144	0.060	0.108	0.510	1.18e+00
25197	5.23	5.24	5.66	5.16	5.16	5.154	5.006	5.154	4.925	0.352	0.172	0.172	1.549	7.30e+00
25790	6.03	5.93	5.61	5.60	5.55	5.558	5.439	5.600	5.543	0.243	0.170	0.396	3.694	3.14e-01
26453	7.66	7.26	6.47	6.29	6.28	6.263	6.186	6.215	5.317	0.124	0.117	0.128	0.406	3.09e-01
26966	5.72	5.73	5.79	5.84	5.78	5.806	5.728	5.631	4.559	0.195	0.110	0.313	0.511	4.90e+00
27072	4.07	3.59	2.80	2.61	2.51	3.085	2.392	2.261	2.394	4.396	0.981	0.228	0.483	2.42e-30
27288	3.65	3.55	3.39	3.31	3.29	3.347	2.991	3.221	2.388	2.115	1.157	0.365	1.001	1.94e-01
27321	4.02	3.85	3.67	3.54	3.53	3.484	3.182	2.597	0.014	3.459	9.047	19.900	11.280	1.61e+00
27980	8.28	7.65	6.49	6.23	6.15	6.169	6.069	6.170	6.084	0.169	0.150	0.940	14.910	2.51e-02
28103	4.05	3.71	3.06	2.98	2.99	2.021	1.749	2.905	2.792	2.878	0.726	0.212	1.648	3.72e-01
28230	7.83	7.55	7.01	6.93	6.88	6.851	6.853	6.834	5.708	0.087	0.061	0.193	0.435	3.54e-01
32480	5.82	5.24	4.41	4.07	4.13	3.872	3.439	3.954	3.825	1.463	0.412	0.381	1.020	5.04e+00
32775	6.57	6.11	5.30	5.13	5.02	5.003	4.794	5.053	4.990	0.391	0.084	0.183	1.643	6.71e-02
33690	7.60	6.81	5.46	5.10	4.99	4.959	4.698	4.980	4.672	0.400	0.267	0.180	1.137	4.66e-02
34276	6.51	6.52	6.49	6.48	6.48	6.486	6.411	6.489	5.853	0.124	0.097	0.203	0.940	1.73e-01
34819	6.25	5.85	5.20	4.98	4.83	4.904	4.661	4.877	4.771	0.551	0.109	0.151	0.699	7.91e-01
35550	3.87	3.50	2.82	2.60	2.56	1.491	1.004	2.622	2.526	3.903	0.834	0.256	0.622	7.28e-02
36906	8.34	7.68	6.49	6.23	6.16	6.135	6.036	6.145	6.053	0.176	0.135	0.145	0.567	1.44e-05
36948	8.96	8.23	6.91	6.58	6.46	6.448	6.369	6.416	5.644	0.357	0.250	0.613	9.612	5.86e-01
39757	3.29	2.83	2.17	2.08	2.02	–0.227	–0.061	1.961	1.856	7.199	1.757	0.397	1.145	2.84e-01
40938	7.64	7.24	6.34	6.15	6.09	6.089	5.932	6.097	5.986	0.168	0.149	0.165	1.297	3.09e-03
41152	5.64	5.52	5.25	5.29	5.25	5.255	5.092	5.270	4.838	0.372	0.140	0.177	0.494	5.09e-02
41307	3.90	3.91	4.12	4.09	4.08	3.927	3.556	3.925	3.429	1.087	0.394	0.280	1.874	2.86e+00
42028	5.81	5.80	5.77	5.82	5.73	5.795	5.707	5.819	5.697	0.202	0.129	0.144	0.593	4.20e-04
42430	5.77	5.05	4.05	3.59	3.59	3.446	3.183	3.480	3.405	1.784	0.380	0.151	0.549	3.10e+00
43970	5.37	5.22	4.91	4.97	4.87	4.894	4.527	4.927	4.593	0.470	0.223	0.319	0.796	1.97e-01
44001	5.89	5.68	5.27	5.21	5.16	5.158	4.978	5.195	4.886	0.324	0.235	0.391	1.386	9.43e-02
45758	6.88	6.62	6.15	6.04	5.96	6.032	5.886	6.015	5.917	0.216	0.118	0.192	0.586	1.44e-04
48164	7.43	7.20	6.75	6.68	6.63	6.637	6.611	6.666	6.177	0.119	0.136	0.243	0.628	1.60e-01
48541	7.75	7.59	7.21	7.20	7.19	7.095	7.164	7.103	6.071	0.113	0.128	0.193	0.487	7.59e-01

Table 1 *Continued.*

HIP	B	V	J	H	K	w1m	w2m	w3m	w4m	f12	f25	f60	f100	χ^2
	mag	mag	mag	mag	mag	mag	mag	mag	mag	Jy	Jy	Jy	Jy	
(1)	(2)	(3)	(4)	(5)	(6)	(7)	(8)	(9)	(10)	(11)	(12)	(13)	(14)	(15)
51438	4.76	4.72	4.75	4.71	4.57	4.555	4.348	4.609	4.531	0.606	0.155	0.145	1.092	2.11e+00
51658	4.94	4.72	4.12	4.06	4.20	4.121	3.875	4.210	4.169	0.919	0.185	0.397	0.955	3.04e+00
52462	8.59	7.72	6.18	5.77	5.66	5.613	5.509	5.629	5.556	0.219	0.083	0.248	0.984	8.08e-02
53524	7.59	7.36	6.91	6.87	6.79	6.717	6.745	6.692	5.475	0.281	0.250	0.601	1.830	2.01e+00
53910	2.37	2.34	2.27	2.36	2.29	1.156	0.845	2.461	2.138	4.795	1.387	0.627	1.000	3.98e+00
53911	11.64	10.92	8.22	7.56	7.30	7.009	6.878	4.540	1.516	0.613	2.435	4.105	4.900	1.78e+00
55505	10.04	8.89	6.40	5.76	5.59	5.496	5.344	3.110	0.202	1.981	9.443	7.895	4.565	5.34e-02
56253	6.38	6.12	5.66	5.60	5.56	5.589	5.435	5.604	5.435	0.243	0.114	0.141	0.863	3.59e-01
56675	6.00	5.64	4.97	4.92	4.70	4.718	4.483	4.698	4.606	0.568	0.250	0.275	7.545	8.22e-01
57632	2.23	2.14	1.85	1.93	1.88	0.461	0.129	2.056	1.698	7.067	2.323	1.027	1.120	7.91e+00
60074	7.64	7.04	5.87	5.61	5.54	5.522	5.357	5.540	5.182	0.259	0.135	0.705	0.909	1.73e-01
61174	4.69	4.30	3.61	3.37	3.37	2.685	2.912	3.308	2.752	2.242	0.770	0.308	0.803	1.56e-01
61498	5.78	5.78	5.78	5.79	5.77	5.368	5.399	5.024	1.222	0.433	3.379	7.359	3.814	1.69e+00
61782	8.14	7.99	7.64	7.59	7.58	7.523	7.564	7.053	3.913	0.094	0.266	0.368	1.155	1.53e-29
61960	4.96	4.88	4.99	4.76	4.68	4.649	4.298	4.700	4.259	0.547	0.235	0.270	0.579	2.64e+00
63584	6.44	6.01	5.19	5.05	5.00	4.983	4.757	5.033	4.914	0.362	0.150	0.130	0.424	6.06e-01
64375	6.68	6.49	6.12	6.02	6.01	5.980	5.906	6.014	5.631	0.196	0.182	0.330	0.796	6.75e-02
64921	7.28	7.07	6.65	6.59	6.57	6.634	6.303	6.435	6.529	0.116	0.062	0.192	1.779	3.37e+00
68101	6.78	6.00	4.57	4.02	3.99	4.008	3.792	4.020	3.965	1.047	0.194	0.382	10.230	1.81e-01
68593	7.72	7.16	6.16	5.94	5.88	5.882	5.794	5.883	5.701	0.187	0.079	0.150	0.305	1.85e-04
69682	9.56	8.89	7.65	7.38	7.27	7.166	7.250	7.230	6.678	0.133	0.128	0.207	0.404	5.72e-01
69732	4.27	4.18	3.98	4.03	3.91	3.922	3.758	4.118	3.611	1.151	0.356	0.472	1.000	3.74e+00
70090	4.02	4.05	4.11	3.98	4.07	4.063	3.851	4.092	3.914	0.953	0.313	0.171	1.233	3.46e-02
70344	7.80	7.21	6.12	5.87	5.79	5.816	5.714	5.773	5.274	0.185	0.089	0.182	0.586	1.89e-01
70952	6.53	6.10	5.26	5.09	5.01	5.447	5.194	5.965	5.151	0.349	0.084	0.344	0.525	1.78e+00
71075	3.23	3.04	2.65	2.57	2.51	1.378	1.247	2.621	2.470	3.937	0.980	0.366	0.496	1.87e+00
71284	4.83	4.47	3.56	3.46	3.34	3.478	3.146	3.507	3.444	1.606	0.413	0.140	0.452	1.78e+00
73049	5.37	5.32	5.22	5.22	5.13	5.173	5.010	5.193	5.031	0.332	0.155	0.190	1.342	5.66e-02
73145	8.07	7.88	7.60	7.56	7.52	7.514	7.523	6.922	4.273	0.156	0.186	0.684	1.324	6.53e-29
73473	4.91	4.91	4.71	4.71	4.62	4.602	4.405	4.681	4.584	0.623	0.282	0.141	0.974	5.57e-02
73512	10.17	9.13	7.19	6.69	6.58	6.577	6.555	6.572	6.527	0.123	0.122	0.130	0.405	9.28e-01
74596	5.34	5.28	5.09	5.15	5.11	5.094	4.926	5.150	4.939	0.348	0.100	0.142	0.601	4.97e-02
74946	2.88	2.87	2.52	2.53	2.53	1.597	1.539	2.731	2.732	3.372	0.763	0.416	5.406	1.78e+00
76127	4.01	4.14	4.43	4.47	4.43	4.412	4.133	4.394	4.228	0.623	0.182	0.162	0.452	3.43e-30
76267	2.25	2.22	2.25	2.39	2.21	0.942	0.935	2.263	1.940	5.807	1.686	0.705	0.869	3.12e-01
76375	8.60	7.65	6.01	5.62	5.50	5.698	5.325	5.511	5.466	0.211	0.070	0.142	0.614	1.11e+00
76635	8.05	7.50	6.50	6.25	6.18	6.202	6.130	6.201	5.985	0.199	0.114	0.131	0.936	7.64e-03
76736	6.53	6.45	6.30	6.34	6.27	6.270	6.219	6.160	5.010	0.263	0.250	0.482	4.657	4.30e+00
76829	5.05	4.64	4.02	3.73	3.80	3.681	3.087	3.650	3.521	1.425	0.693	0.661	2.368	4.87e+00
77163	5.61	5.57	5.47	5.46	5.43	5.402	5.258	5.428	4.997	0.330	0.124	0.283	0.920	8.59e+00
77542	7.21	7.11	6.87	6.86	6.82	6.061	6.095	4.701	1.861	0.533	1.819	5.335	3.548	1.78e+00
78554	4.89	4.82	5.01	4.66	4.62	4.647	4.455	4.653	4.574	0.577	0.145	0.190	0.749	3.26e+00
81126	4.19	4.20	4.42	4.34	4.05	4.173	3.903	4.175	4.099	0.937	0.270	0.265	0.651	4.49e+00
81641	5.77	5.77	5.75	5.79	5.74	5.824	5.712	5.792	5.340	0.207	0.111	0.226	1.189	3.55e-02
81800	7.02	6.48	5.44	5.17	5.15	5.168	4.994	5.166	5.023	0.321	0.073	0.116	0.640	1.02e-01
82405	6.72	6.32	5.46	5.29	5.18	5.188	5.019	5.202	5.123	0.381	0.262	0.295	1.148	8.22e-02
83480	6.89	6.70	6.30	6.25	6.22	6.190	6.092	6.190	6.048	0.156	0.104	0.321	2.245	1.96e-01
85157	5.93	5.70	5.24	5.21	5.18	5.178	5.028	5.167	4.018	0.356	0.212	0.536	1.086	2.54e-01
85537	5.65	5.41	4.81	4.88	4.80	4.777	4.572	4.802	4.599	0.572	0.258	0.366	2.093	2.38e-01
87108	3.79	3.75	3.59	3.66	3.62	3.677	3.356	3.646	3.118	1.417	0.525	1.269	3.733	1.21e-05
87558	6.20	5.77	5.21	4.83	4.71	4.737	4.453	4.717	4.576	0.544	0.250	0.380	1.265	3.00e+00
88399	7.47	7.01	6.16	6.02	5.91	5.758	5.703	5.799	4.940	0.208	0.158	0.647	2.631	2.83e+00
90185	1.76	1.79	1.73	1.77	1.77	–0.704	–0.165	1.763	1.681	8.460	2.047	0.586	2.616	7.25e-01
90936	6.65	6.22	5.42	5.28	5.20	5.206	5.053	5.224	5.082	0.292	0.139	0.504	1.029	1.32e-01
91262	0.03	0.03	–0.18	–0.03	0.13	–2.034	–2.082	0.017	–0.157	41.530	11.310	9.568	7.912	9.42e-02
92024	4.98	4.78	4.38	4.25	4.30	4.335	4.065	3.624	2.355	1.518	1.092	0.306	0.991	8.61e-30
93542	4.71	4.74	4.72	4.96	4.75	4.794	4.526	4.723	3.792	0.577	0.306	0.321	1.119	6.98e-01
95261	5.05	5.03	5.10	5.15	5.01	5.059	4.822	4.725	3.261	0.481	0.491	0.495	0.435	1.45e-29
95270	7.52	7.04	6.20	5.98	5.91	5.887	5.810	5.894	3.952	0.164	0.248	1.855	1.719	1.51e-01
95619	5.65	5.66	5.67	5.66	5.68	5.677	5.559	5.612	4.579	0.190	0.199	0.412	0.942	1.79e+00
96468	4.28	4.36	4.44	4.42	4.48	4.549	4.256	4.593	4.511	0.609	0.166	0.265	1.804	8.80e-01
99273	7.66	7.18	6.32	6.09	6.08	6.062	5.882	5.995	4.056	0.111	0.339	0.711	0.328	1.96e-03
99473	3.17	3.24	3.29	3.28	3.29	3.390	3.024	3.435	3.350	1.745	0.447	0.204	0.941	1.78e+00
101612	5.04	4.75	4.28	4.02	4.04	4.060	3.582	4.045	3.865	1.016	0.264	0.522	1.798	3.38e-01
101769	4.07	3.64	2.87	2.76	2.64	1.584	0.844	2.634	2.518	4.069	0.921	0.229	1.066	8.24e-02

Table 1 *Continued.*

HIP	B	V	J	H	K	w1m	w2m	w3m	w4m	f12	f25	f60	f100	χ^2
	mag	mag	mag	mag	mag	mag	mag	mag	mag	Jy	Jy	Jy	Jy	
(1)	(2)	(3)	(4)	(5)	(6)	(7)	(8)	(9)	(10)	(11)	(12)	(13)	(14)	(15)
101800	5.47	5.42	5.41	5.37	5.30	5.324	5.134	5.326	4.968	0.251	0.124	0.177	1.077	8.79e-01
102409	10.28	8.81	5.44	4.83	4.53	4.499	3.999	4.312	4.137	0.760	0.300	0.270	0.687	1.13e-02
103752	6.46	6.36	6.13	6.11	6.05	6.056	5.921	6.085	6.121	0.146	0.103	0.244	0.638	2.07e-03
105570	5.22	5.16	5.09	4.98	4.92	4.885	4.699	4.966	4.793	0.459	0.251	0.274	1.925	3.40e-01
106741	7.59	7.19	6.38	6.25	6.18	6.192	6.066	6.185	5.927	0.159	0.113	0.199	0.520	7.66e-02
107022	7.83	7.07	5.73	5.41	5.27	5.309	5.121	5.306	5.209	0.315	0.107	0.174	0.987	1.23e-02
107412	7.13	6.69	5.87	5.69	5.59	5.573	5.452	5.629	5.481	0.249	0.194	0.228	0.491	1.02e-02
107649	6.17	5.57	4.72	4.31	4.24	4.116	3.817	4.156	4.065	0.805	0.216	0.245	1.000	5.01e+00
108809	7.13	6.63	5.70	5.44	5.39	5.338	5.180	5.393	5.251	0.287	0.152	0.137	0.680	1.33e-01

Col.(1): *Hipparcos* identification. Col.(2): *B* magnitude. Col.(3): *V* magnitude. Col.(4): *J* magnitude. Col.(5): *H* magnitude. Col.(6): *K* magnitude. Col.(7): *WISE* W1 magnitude. Col.(8): *WISE* W2 magnitude. Col.(9): *WISE* W3 magnitude. Col.(10): *WISE* W4 magnitude. Col.(11): *IRAS* 12 μm flux density. Col.(12): *IRAS* 25 μm flux density. Col.(13): *IRAS* 60 μm flux density. Col.(14): *IRAS* 100 μm flux density. Col.(15): The minimum χ^2 of SED fittings.
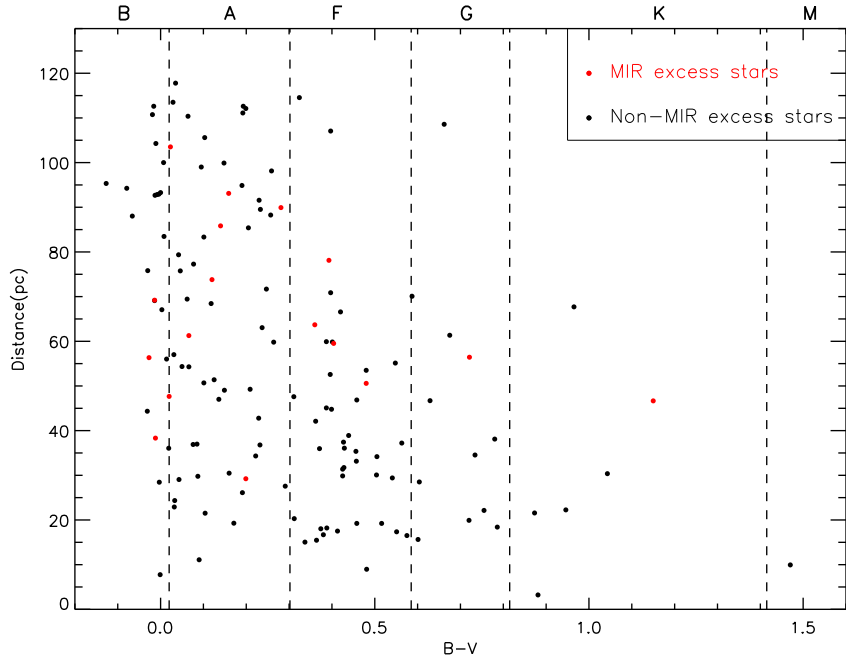
Fig. 1 Distribution of Mid-IR excess sample and Non Mid-IR excess sample stars in distance from Earth as a function of $B - V$.

all 143 sample stars by using the criterion [F_{IRAS} - F_{phot}] / $\sigma_{IRAS} > 3.0$, where F_{IRAS} is the *IRAS* flux densities; F_{phot} is the predicted photospheric flux densities of corresponding bands; and σ_{IRAS} is the uncertainties of the *IRAS* flux densities in corresponding bands.

3.1 *WISE* 22 μm Excess

The observation data of *WISE* will be used to search Mid-IR excess objects. All 143 stars are covered by *WISE*. While our previous work showed that the model fluxes at *WISE* 12 and 22 μm have the systematical uncertainties σ_{sys} with $\sigma_{w3} = 0.06$ and $\sigma_{w4} = 0.13$ (Liu et al. 2014). Therefore, the systematical uncertainty should be considered to the uncertainties of *WISE* all bands σ_{WISE}

with $\sigma_{WISE} = \sqrt{\sigma_{obs}^2 + \sigma_{sys}^2}$, where σ_{obs} means the observational uncertainties of *WISE*. Note that three stars (HIP 70952, HIP 71284, HIP 74946) were removed from the sample with [F_{w4obs} - F_{w4phot}] $< -1 * \sigma_{w4}$ where F_{w4obs} is the *WISE* 22 μm flux density and F_{w4phot} is the predicted photospheric flux density at 22 μm band. Therefore, there are 140 stars left in our sample for further discussion. These 140 stars' *WISE* magnitudes information can be seen from Table 1.

The flux densities of $W1$ and $W2$ can be used to test the fitting quality of model spectra. The flux densities of $W3$ and $W4$ can be used to fit the dust components and revise the dust properties of the stars in Rhee et al. (2007).
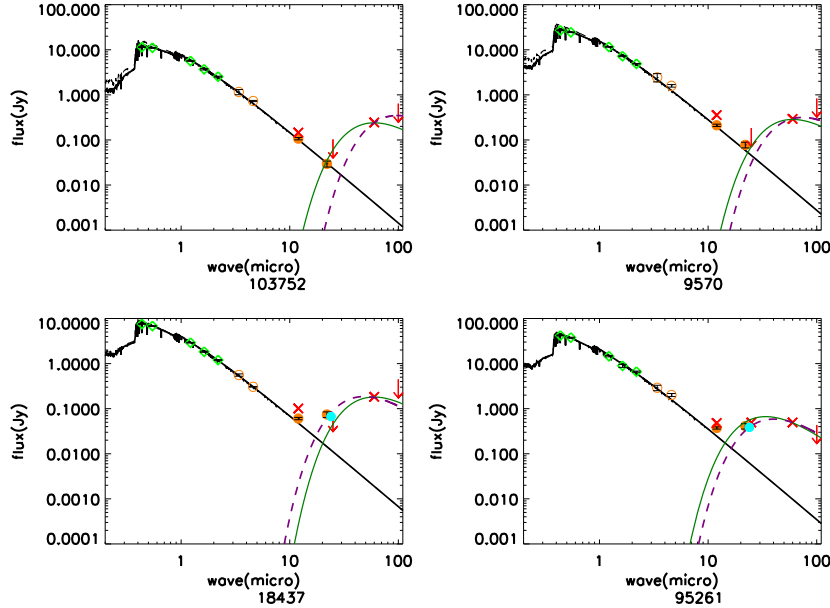
Fig. 2 SEDs for four IR excess stars. The photospheric models and the disk models are shown as *solid black* and *dotted purple lines*, respectively. The *green solid lines* are the disk models of Rhee. The different symbols represent the different data sets: *green diamonds*, *BVJHK*; *red*, *IRAS*; *cyan filled dots*, *Spitzer*; *orange filled dots*, *WISE* without saturations; and *orange hollow circles*, *WISE* with saturations.
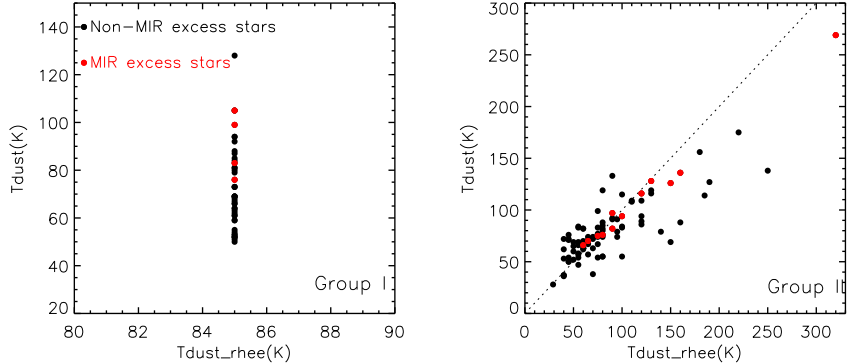
Fig. 3 The differences of dust temperatures between Rhee et al. (2007) and ours. Group I and Group II stars are shown in the left and right panels, respectively. The different symbols represent the different sub-sample stars: *red filled dots* are MIR excess stars and *black filled dots* are the Non-MIR excess stars.

We can estimate the Mid-IR excesses at *WISE* 22 μm in the same way as 60 μm excess shown:

$$[F_{w4\text{obs}} - F_{w4\text{phot}}] / \sigma_{w4} > 3.0,$$

We identify 31 stars with excesses at the 22 μm by applying this criterion. While this criterion is affected by the *IRAS* 100 μm background, whose level should be lower than 5 MJy sr^{-1} as Kennedy & Wyatt (2012) and Wu et al. (2013) shown. We check the 31 μm excess stars and find indeed there are 14 stars that may be affected. So there are only 17 stars left after this cut. Mid-IR excess stars are thought to have co-existence of hot and cold dust components just like our solar system. These 17 stars are

put into the Mid-IR excess sample which are listed in Table 2. At the following sections, I will discuss these two sub-samples: Mid-IR excess sample and Non Mid-IR excess sample.

3.2 Properties of Debris Disk Host stars

In this subsection, I will study the stellar properties of debris disk hosts including color, distance from the Earth and location on the H-R diagram. Debris disk host stars are more inclined to early type stars as Rhee et al. (2007) pointed out which can be seen from the figure of sample stars function distribution of the distance from Earth and
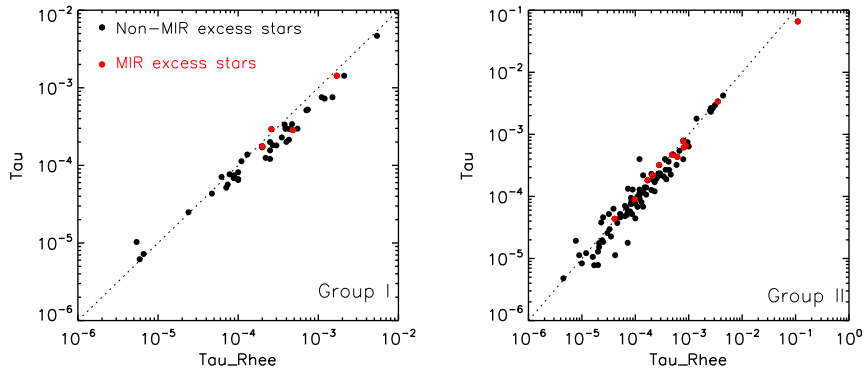
Fig. 4 The differences of fractional luminosities between Rhee et al. (2007) and ours. Group I and Group II stars are shown in the left and right panels, respectively. The different symbols represent the different sub-sample stars: *red filled dots* are MIR excess stars and *black filled dots* are the Non-MIR excess stars.

$B - V$. We re-draw the figure and mark the Mid-IR excess objects in red dots as Figure 1 shown. From the figure, we can see the Mid-IR excess sample has smaller distribution of distance from Earth (29.2 pc to 103.5 pc) than the Non Mid-IR excess sample stars (3.2 pc to 117.8 pc). Note that there are only 17 Mid-IR excess stars, the sample is so small that may lead to a false distribution trend.

3.3 Dust Properties

In this subsection, I will study the dust properties including the dust temperatures and fractional luminosities of debris disks.

3.3.1 Dust temperatures

Debris disks usually consist of a single narrow ring which reach thermal equilibrium in the field of stellar radiation as previous studies suggested (Backman & Paresce 1993). Rhee et al. (2007) used the blackbody model with single-temperature to fit the dust component and obtained dust temperature T for each star.

Since the *IRAS* sample of Rhee is based on solely *IRAS*, the dust properties of 45 objects in their sample still cannot be determined due to the limitations with the *IRAS* database (have *IRAS* detection at 60 μm only). They set the dust temperature to 85 K so the peak will fall at 60 μm. According to the number of the *IRAS* detected bands, I divide the 140 stars sample into two groups:

(1) Group I contains 45 stars with only *IRAS* 60 μm detection;

(2) Group II contains the remaining 95 stars with multi-band *IRAS* detections.

The excessive flux densities are fitted in IR bands including 60, 100 μm of *IRAS* and 12, 22 μm of *WISE* with a blackbody model of single temperature. The SED fittings of four stars as an example are presented in Figure 2. From

SED fittings, the dust temperatures can be derived with group I stars listed in Table 3 and Group II stars listed in Table 4. From the figure, one can easily see that our fitting results are better than Rhee's because of the addition of new *WISE* data.

3.3.2 Fractional luminosities

From the SED fitting, we can also estimate the fractional luminosity f which is used to characterize the disk's effective optical depth. The fractional luminosity f is calculated by dividing the IR luminosity of debris disk to the stellar luminosity (Wyatt 2008),

$$f = L_{\mathrm{ir}}/L_{\star}, \tag{1}$$

where $L_{\star}$ is the stellar luminosity estimated by the best model of SED fitting. The IR luminosity L_{ir} is calculated from the blackbody model of fitted IR. The calculated fractional luminosities for all sample stars are also listed in Table 3 and Table 4.

4 DISCUSSION

In this section, I will first give my discussion on revising the dust properties including dust temperatures and fractional luminosities. I will then discuss the Mid-IR excess sample.

4.1 Revising the Dust Temperatures

The revised dust temperature can be seen in Table 3 and Table 4. For Group I stars, we can get the dust temperatures which were set to 85 K in Rhee et al. (2007). For Group II stars, even they have multi-band *IRAS* detections, the dust temperatures of ours are well determined than that in Rhee et al. (2007) because of the much better sensitivity in the Mid-IR of *WISE* in comparison with *IRAS*.

Table 2 The List of *WISE* 22 μm Excess Stars

HIP (1)	Mid-IR excess (2)	References (3)
5626	no	
7345	yes	[1],[2],[3],[4]
11847	yes	[2],[3],[5]
16449	yes	[2]
18437	yes	[2]
22226	yes	[2],[5]
23451	no	[3],[5]
24528	yes	[2]
26453	yes	[2],[5]
26966	yes	[2]
27288	no	
27321	no	[1],[3],[4]
28230	yes	[2]
36948	no	[5]
41307	yes	
48541	yes	[2]
53524	no	[3]
53911	yes	
55505	yes	[1],[3]
61498	no	[1],[3]
61782	no	[1],[4]
73145	no	[3],[5]
76736	no	[3],[5]
85157	no	
88399	no	[3]
92024	yes	[4]
93542	yes	[2]
95261	yes	[1],[2]
95270	yes	[2],[3],[5]
99273	no	[3]
116431	no	[2]

Col.(1): *Hipparcos* identification. Col.(2): Check the 22 μm excess by *IRAS* 100 μm background level lower than 5 MJy sr^{-1} or not, yes means the excess should be true and no means the excess may not be true. Col.(3): References - [1] Fujiwara et al. (2013); [2] Wu et al. (2013); [3] Liu et al. (2014); [4] Ishihara et al. (2017); [5] Ballering et al. (2018).

The difference of dust temperatures between Rhee et al. (2007) and ours is shown in Figure 3. From Figure 3, we can see the dust temperatures of Group II stars are overestimated in the high temperature band. While in lower temperature band (<100 K), dust temperatures have a part underestimated and a part overestimated, which have no obvious favoritism.

4.2 Revising the Fractional Luminosities

The differences of fractional luminosities *f* between Rhee et al. (2007) and ours are shown in Figure 4. It is obvious that the fractional luminosities of Group I stars are high estimated by Rhee due to the high estimated dust temperatures which can be seen from the left panel of Figure 4. While for Group II stars, the fractional luminosities show no obvious favoritism with a part under estimated and a part over estimated which can be seen from the right panel of Figure 4. However, for the Mid-IR excess sample stars in this group, fractional luminosities of mine are almost the same as Rhee et al. (2007). It is most likely

Table 3 The Dust Properties of Group I Stars

HIP (1)	*T*-Rhee(K) (2)	*f*-Rhee (3)	*T*(K) (4)	*f* (5)
4267	85	8.80e-05	73	7.13e-05
6686	85	5.90e-06	105	6.17e-06
8122	85	4.70e-04	66	3.40e-04
9570	85	1.00e-04	69	8.16e-05
11486	85	1.10e-04	85	1.13e-04
11847	85	1.70e-03	83	1.43e-03
13005	85	1.10e-03	52	7.56e-04
18437	85	2.60e-04	105	2.93e-04
18859	85	1.30e-04	94	1.38e-04
18975	85	8.90e-05	69	7.45e-05
20635	85	4.70e-05	81	4.33e-05
23451	85	5.40e-03	87	4.68e-03
25790	85	2.50e-04	55	1.21e-04
26966	85	2.00e-04	99	1.76e-04
34276	85	2.00e-04	73	1.72e-04
36906	85	4.30e-04	50	2.95e-04
39757	85	5.40e-06	128	1.03e-05
40938	85	3.50e-04	53	2.29e-04
42028	85	7.10e-05	59	5.16e-05
43970	85	1.00e-04	73	6.48e-05
44001	85	2.20e-04	66	1.25e-04
45758	85	2.70e-04	51	1.82e-04
48164	85	5.50e-04	63	2.97e-04
48541	85	4.80e-04	76	2.85e-04
51438	85	2.40e-05	79	2.49e-05
53524	85	1.50e-03	69	7.55e-04
56253	85	1.00e-04	61	6.66e-05
61960	85	6.20e-05	94	7.11e-05
64375	85	3.90e-04	64	3.04e-04
69682	85	2.10e-03	62	1.43e-03
70344	85	3.80e-04	80	3.36e-04
73049	85	7.40e-05	67	5.67e-05
73512	85	1.20e-03	54	7.25e-04
76635	85	3.90e-04	64	2.96e-04
82405	85	3.00e-04	53	1.81e-04
83480	85	4.30e-04	52	2.14e-04
87108	85	7.80e-05	81	7.68e-05
87558	85	2.50e-04	69	2.00e-04
95619	85	2.00e-04	88	1.71e-04
99473	85	6.60e-06	92	7.22e-06
103752	85	2.50e-04	52	1.56e-04
105570	85	8.80e-05	68	6.86e-05
106741	85	4.00e-04	61	2.01e-04
110867	85	7.10e-04	59	5.13e-04
116431	85	7.40e-04	84	5.23e-04

Col.(1): *Hipparcos* identification. Col.(2): Dust temperatures of Rhee. Col.(3): Fractional luminosities of Rhee. Col.(4): The revised dust temperatures of this paper. Col.(5): The revised fractional luminosities of this paper.

because they have plenty of IR excess data to do blackbody fittings.

Whether in Group I or Group II, Mid-IR sample stars have higher fractional luminosities than Non Mid-IR sample stars, which imply that the stars with higher fractional luminosities may have higher probability of having warm dust component.

4.3 Mid-IR Excess Sample (*WISE* 22 μm)

From Section 3, Mid-IR excess sample contains 17 stars with *WISE* 22 μm excesses. Such stars with

Table 4 The Dust Properties of Group II Stars

HIP	T-Rhee(K)	f-Rhee	T(K)	f
746	120	2.50e-05	109	1.85e-05
1185	40	4.30e-04	36	2.67e-04
5626	75	1.50e-04	83	1.40e-04
6878	45	2.10e-04	50	1.88e-04
7345	80	7.90e-04	76	7.90e-04
7805	70	3.70e-04	74	2.69e-04
7978	65	4.20e-04	68	3.63e-04
8241	75	6.40e-05	76	7.03e-05
10054	60	8.70e-05	66	5.20e-05
10670	75	7.20e-05	74	5.57e-05
11360	65	5.10e-04	68	4.74e-04
12361	40	5.90e-04	37	3.22e-04
12964	55	2.00e-04	54	1.27e-04
13141	55	6.40e-05	83	4.81e-05
14576	250	1.70e-05	138	7.79e-06
15197	95	2.50e-05	79	4.61e-05
16449	60	4.90e-04	66	4.71e-04
16537	40	8.30e-05	53	7.52e-05
19893	80	2.30e-05	74	3.81e-05
21604	75	3.80e-04	54	1.89e-04
22226	65	8.80e-04	70	6.51e-04
22439	40	2.30e-04	62	1.21e-04
22845	80	8.40e-05	88	8.24e-05
24528	100	1.70e-04	94	1.82e-04
25197	120	7.00e-05	86	5.06e-05
26453	90	2.80e-04	97	3.21e-04
27072	90	7.70e-06	133	1.93e-05
27288	220	1.30e-04	175	8.09e-05
27321	110	2.60e-03	109	2.65e-03
27980	70	2.80e-03	38	2.62e-03
28103	185	2.00e-05	114	1.29e-05
28230	90	6.10e-04	82	4.35e-04
32480	60	8.90e-05	82	1.29e-04
32775	45	1.60e-04	54	1.07e-04
33690	80	2.00e-04	82	2.31e-04
34819	45	1.00e-04	72	7.69e-05
35550	60	8.90e-06	82	1.13e-05
36948	60	2.60e-03	63	2.31e-03
41152	80	5.20e-05	85	5.23e-05
41307	130	4.10e-05	128	4.36e-05
42430	80	3.20e-05	119	5.21e-05
51658	40	1.10e-04	37	6.79e-05
52462	45	6.70e-04	50	5.43e-04
53910	120	1.20e-05	94	1.22e-05
55505	160	1.10e-01	136	6.59e-02
56675	50	1.40e-04	65	6.84e-05
57632	160	4.20e-05	88	1.13e-05
60074	55	9.50e-04	57	7.47e-04
61174	180	1.20e-04	156	1.05e-04
61498	110	4.40e-03	108	4.22e-03
61782	130	2.50e-03	119	2.41e-03
63584	100	1.00e-04	55	4.43e-05
64921	80	3.40e-04	55	2.10e-04
68101	45	2.50e-04	71	1.93e-04
68593	60	1.40e-04	62	2.19e-04
69732	100	5.20e-05	84	4.59e-05
70090	120	2.10e-05	89	1.53e-05
71075	55	1.00e-05	69	8.35e-06
73145	90	3.10e-03	91	2.95e-03
73473	150	7.20e-05	69	1.79e-05
74596	65	3.30e-05	74	2.97e-05
76127	75	2.00e-05	99	7.85e-06
76267	190	2.40e-05	127	1.97e-05
76375	29	7.90e-04	28	3.97e-04
76736	140	1.20e-04	79	3.99e-04
76829	75	1.20e-04	77	1.29e-04
77163	40	1.40e-04	72	1.16e-04
78554	45	4.60e-05	76	3.73e-05

Table 4 *Continued.*

HIP	T-Rhee(K)	f-Rhee	T(K)	f
81126	80	3.00e-05	80	2.57e-05
81641	95	1.20e-04	74	9.24e-05
81800	55	8.30e-05	66	9.49e-05
85157	90	2.70e-04	92	2.14e-04
85537	70	6.80e-05	63	6.52e-05
88399	70	1.00e-03	72	6.40e-04
90185	100	4.50e-06	115	4.80e-06
90936	50	4.60e-04	52	2.25e-04
91262	80	2.10e-05	76	1.77e-05
92024	320	8.10e-04	269	6.18e-04
93542	120	9.70e-05	116	8.99e-05
95261	150	2.10e-04	126	2.17e-04
95270	75	3.50e-03	75	3.38e-03
96468	60	3.50e-05	70	2.26e-05
99273	95	1.40e-03	91	1.79e-03
101612	65	1.10e-04	71	1.00e-04
101769	130	1.60e-05	116	1.06e-05
101800	100	3.90e-05	83	6.34e-05
102409	50	3.60e-04	60	3.99e-04
107022	80	2.90e-04	55	2.35e-04
107412	55	2.70e-04	58	2.33e-04
107649	55	1.20e-04	84	1.12e-04
108809	75	7.30e-05	67	1.33e-04
109857	65	1.60e-04	67	1.39e-04
111278	55	9.30e-05	47	8.48e-05
113368	65	8.00e-05	57	5.72e-05
114189	50	2.30e-04	69	1.70e-04

The explanation of each column is same to Table 3.

Mid-IR excess emission may have terrestrial planets (Padgett & Stapelfeldt 2016).

Up to now, a few hundreds of warm disks with Mid-IR excess have been discovered with *Spitzer*, *AKARI* and *WISE* (Meyer et al. 2008; Fujiwara et al. 2010a,b; Olofsson et al. 2012; Ribas et al. 2012; Fujiwara et al. 2013; Wu et al. 2012, 2013; Liu et al. 2014; Ishihara et al. 2017; Ballering et al. 2018), and such disks' incidence decreases very rapidly with increasing stellar ages (Urban et al. 2012).

What is the cause of the warm component? For most warm debris disks, the Mid-IR excesses could be explained by giant impact stages (about 100 Myr) (Genda et al. 2015). They found that, after a giant impact, the IR excess is sometimes almost 10 times higher than the stellar IR flux.

In Mid-IR excess sample, 15 stars can be found in previous work as shown in column 3 in Table 2. Note that maybe the remaining two stars can be seen in the other work elsewhere.

5 SUMMARY

This paper has refitted the SEDs of the sample stars with the Kurucz' models and refitted the excessive flux densities with *WISE* and *IRAS* all sky catalogs. We obtain the dust temperatures of Group I stars with only 60 μm data which cannot determined in previous study of Rhee. For Group II stars, even they have *IRAS* multi-bands detections,

the dust temperatures of ours are well determined than that in Rhee et al. (2007) because of the much better sensitivity in the Mid-IR of *WISE* in comparison with *IRAS*. From the revised dust properties, we can see that the dust temperatures of Group II stars were overestimated in the high temperature band before and the fractional luminosities of Group I stars were high estimated.

Moreover, we identify 17 stars with *WISE* 22 μm excess and discuss the difference from the Non Mid-IR sample. Disks around the Mid-IR sample stars appear to be brighter and with higher dust temperatures. We hope these revisions of dust properties can give some guidance to the follow-up works.

References

Abraham, P., Leinert, C., Burkert, A., Lemke, D., Henning, T. 1999, A&A, 338, 91

Aumann, H. H., et al. 1984, ApJ, 278, L23

Backman, D. E., & Paresce, F. 1993, in Protostars and Planets III, eds. V. Mannings, A. P. Boss, & S. S. Russell (Tucson: Univ. Arizona Press), 1253

Ballering, N. P., Rieke, G. H., Su, K. Y. L., et al. 2018, VizieR Online Data Catalog, J/ApJ/845/120

Beichman, C. A., Bryden, G., Stapelfeldt, K. R. et al. 2006, ApJ, 652, 1674

Bessell, M. 2000, PASP, 112, 961

Booth, M., Matrà, L., Su, K. Y. L., et al. 2019, MNRAS, 482, 3443

Borgniet, S., Boisse, I., Lagrange, A.-M., et al. 2014, A&A, 561, A65

Bryden, G., et al. 2006, ApJ, 636, 1098

Bulger, J., Hufford, T., Schneider, A., et al. 2013, A&A, 556 , A119

Castelli, F., & Kurucz, R. L. 2004, arXiv:astro-ph/0405087

Chen, C. H., Patten, B. M., Werner, M. W., et al. 2005, ApJ, 634, 1372

Chen, C.H., Mittal, T., Kuchner, M., et al. 2014, ApJS, 211, 25

Cotten, T. H., & Song, I. 2016, ApJS, 225, 15

Cox, A. N., & Pilachowski, C. A. 2000, PhT, 53, 10000

Decin, G., Dominik, C., Waters, L. B. F. M., & Waelkens, C. 2003, ApJ, 598, 636

Dodson-Robinson, S. E., Su, K. Y. L., Bryden, G., et al. 2016, ApJ, 833, 183

Eiroa, C., Marshall, J. P., et al. 2013, A&A, 555, 11

Fajardo-Acosta, S. B., Stencel, R. E., Backman, D. E., & Thakur, N. 1999, ApJ, 520, 215

Fujiwara, H., Yamashita, T., Ishihara, D., et al. 2009, ApJL, 695, L88

Fujiwara, H., Onaka, K., et al. 2010a, ApJ, 714, 152

Fujiwara, H., Ishihara, D., et al. 2010b, cosp, 38, 2470

Fujiwara, H., Ishihara, D., et al. 2013, A&A, 550, 45

Geiler, F., Krivov, A. V., Booth, M., et al. 2019, MNRAS, 483, 332

Genda, H., Kobayashi, H., & Kokubo, E. 2015, ApJ, 810, 136

Greaves, J. S., Holland, W. S., Matthews, B. C., et al. 2016, MNRAS, 461, 3910

Habing, H., Dominik, C., Jourdain de Muizon, M., et al. 1999, Nature, 401, 456

Holland, W. S., Mattews, B. C., Kennedy, G. M., et al. 2017, MNRAS, 470, 3606

Hughes, A. M., Ducheãne, G., & Matthews, B. C. 2018, ARA&A, 56, 541

Hung, L. W., Fitzgerald, M. P., Chen, C. H., et al. 2015, ApJ, 802, 138

Ishihara, D., Takeuchi, N., Kobayashi, H., et al. 2017, A&A, 601, A72

Kawada, M., Baba, H., et al. 2007, PASJ, 59, 389

Kennedy, G. M., & Wyatt, M. C. 2012, MNRAS, 426, 91

Kessler, M. F., Steinz, J. A., et al. 1996, A&A, 315, 27

Kim, J. S., Hines, D. C., Backman, D. E., et al. 2005, ApJ, 632, 659

Konopacky, Q. M., Rameau, J., Duchêne, G., et al. 2016, ApJL, 829, L4

Krivov, A. V. 2010, RAA (Research in Astronomy and Astrophysics), 10, 383

Liu, Q., Wang, T. G., & Jiang, P. 2014, AJ, 148, 3

Marshall, J. P., Krivov, A. V., del Burgo, C., et al. 2013, A&A, 557, A58

Matthews, B. C., Sibthorpe, B., Kennedy, G., et al. 2010, A&A, 518, 135

Maldonado, J., Eiroa, C., Villaver, E., et al. 2012, A&A, 541, A40

Mannings, V., & Barlow, M. J. 1998, ApJ, 497, 330

Meyer, M. R., et al. 2008, ApJL, 673, L181

Mittal, T., Chen, C.H., Jang-Condell, H., et al. 2015, ApJ, 798, 87

Moór, I., Abraham, P., Derekas, A., et al. 2006, ApJ, 644, 525

Moór, I., Pascucci, A., et al. 2011, ApJS, 193, 4

Moór, A., Curé, M., Kóspál, Á., et al. 2017, ApJ, 849, 123

Neugebauer, G., Habing, H. J., et al. 1984, ApJ, 278, 1

Nilsson, R., Liseau, R., Brandeker, A., et al. 2010, A&A, 518, A40

Olofsson, J., Juhász, A., et al. 2012, A&A, 542, 90

Oudmaijer, R. D., van der Veen, W. E. C. J., et al. 1992, A&A, 96, 625

Padgett, D., & Stapelfeldt, K. 2016, Young Stars & Planets Near the Sun, 175

Rebull, L. M., et al. 2008, ApJ, 681, 1484

Rhee, J. H., Song, I. R., Zuckerman, B., & McElwain, M. 2007, ApJ, 660, 1556

Ribas, A، Meriń, B., et al. 2012, A&A, 541, 38

Rieke, G. H., Young, E. T., Engelbracht, C. W., et al. 2004, ApJS, 154, 25

Rieke, G. H., et al. 2005, ApJ, 620, 1010

Rodriguez, D. R., & Zuckerman, B. 2012, ApJ, 745, 147

Sibthorpe, B., Kennedy, G. M., Wyatt, M. C., et al. 2018, MNRAS, 475, 3046

Siegler, N., Muzerolle, J., Young, E. T., et al. 2007, ApJ, 654, 580

Skrutskie, M. F., Cutri, R. M., Weinberg, M. D., et al. 2006, AJ, 131, 1163

Spangler, C., et al. 2001, ApJ, 555, 932

Su, K. Y. L., Rieke, G. H., Stansberry, J. A., Bryden, G., et al. 2006, ApJ, 653, 675

Su, K. Y. L., Morrison, S., Malhotra, R., et al. 2015, ApJ, 799, 146

Urban, L. E., Rieke, G., et al. 2012, ApJ, 750, 98

Vican, L., & Schneider, A. 2014, ApJ, 780, 154

Vican, L., Schneider, A., Bryden, G., et al. 2016, ApJ, 833, 263

Welsh, B. Y., & Montgomery, S. L. 2018, MNRAS, 474, 1515

Werner, M. W., Roellig, T. L., Low, F. J., et al. 2004, ApJS, 154, 1

Wright, E. L., et al. 2010, AJ, 140, 1868

Wu, C. J., Wu, H., Lam, M. I., et al. 2013, ApJS, 208, 29

Wu, C. J., Wu, H., Liu, K., et al. 2016, RAA (Research in Astronomy and Astrophysics), 16, 102

Wu, H., Wu, C. J., & Cao, C. 2012, RAA (Research in Astronomy and Astrophysics), 12, 513

Wyatt, M. C., Smith, R., Su, K. Y. L., et al. 2007, ApJ, 663, 365

Wyatt, M. C. 2008, ARA&A, 46, 339

Wyatt, M. C., Bonsor, A., Jackson, A. P., et al. 2017, MNRAS, 464, 3385

Wyatt, M. C. 2018, Handbook of Exoplanets, 146

Yamamura, S., et al. 2010, cosp, 38, 2496Y